Mild-hydrothermal synthesis of $RE(OH)SO_4$ layered compounds (RE = La-Tb), crystal structure, thermolysis, and photoluminescence

Fan Li,[a] Zhiyuan Pan,[a] Sihan Feng,[a] Qi Zhu,[a] Xudong Sun,[a] Ji-Guang Li[b,*]

[a] *Key Laboratory for Anisotropy and Texture of Materials (Ministry of Education), School of Materials Science and Engineering, Northeastern University, Shenyang, Liaoning 110819, China*

[b] *Research Center for Electronic and Optical Materials, National Institute for Materials Science, Tsukuba, Ibaraki 305-0044, Japan*

[*]Corresponding author

Dr. Ji-Guang Li

National Institute for Materials Science

Tel: +81-29-860-4394

E-mail: li.jiguang@nims.go.jp

Abstract

A series of $RE(OH)SO_4$ layered compounds (RE = La-Tb lanthanides) were successfully synthesized via hydrothermal reaction under near-neutral solution pH and the mild temperature of 180 °C for 24 h, and the temperature/pH/time courses of phase/morphology evolution were clarified with RE = Tb for example. The compounds were characterized in detail for crystallite morphology, crystal structure, thermal behavior and vibrational property, and the intrinsic influence of lanthanide contraction was unveiled. $Tb(OH)SO_4$ was analyzed to be isostructural with its La-Gd analogues (CN = 9 for Tb), instead of the reportedly Dy-Yb ones (CN = 8), and have parameters of a = 4.3806 Å, b = 12.1729 Å, c = 6.7674 Å and β = 106.3967° for its monoclinic unit cell ($P2_1/n$ space group). The Eu and Tb compounds exhibited red (λ_{ex} = 395 nm, λ_{em} = 616 nm) and green (λ_{ex} = 369 nm, λ_{em} = 545 nm) emissions, and have fluorescence lifetimes of ~0.84 and 1.07 ms and chromaticity coordinates of around (0.632, 0.365) and (0.295, 0.481), respectively.

***Keywords**:* $RE(OH)SO_4$; Crystal structure; Hydrothermal crystallization; Phase/morphology evolution

1. Introduction

Layered rare earth hydroxides (LREH) received broad research interest because of their peculiar layered structure, rich interlayer chemistry and abundant functionalities of the RE elements. Typical examples of this category of compounds may include $RE(OH)_2A$, where A is NO_3^- or a halogen anion [1-3], $RE_2(OH)_5A{\cdot}nH_2O$ (A^--LREH, n ~ 1.5) [4-6], $RE_2(OH)_4SO_4{\cdot}nH_2O$ (SO_4^{2-}-LREH, n = 0 or 2) [7-9] and $RE(OH)SO_4$ [10]. $RE(OH)SO_4$ received attention due to its potential applications in catalysis and electrical/optical devices [10, 11]. For example, Ce doped $La(OH)SO_4$ was suggested to be a promising black light radiation material for insect killing [12, 13]. Meanwhile, with rising importance of the sacrificial template method for materials synthesis, $RE(OH)SO_4$ can be a precursor better than the aforesaid SO_4^{2-}-LREH and A^--LREH for RE fluorides, phosphates, vanadates, molybdates, tungstates and so on, due to its lower OH^-/RE^{3+} molar ratio [14-16]. This is because the released excessive OH^- would compete with the anions in the targeted compound for RE^{3+} coordination, which reduces the kinetics of phase conversion and even causes an incomplete reaction [16, 17].

The crystal structure $RE(OH)SO_4$ has been studied by several individual research groups. For example, Haschke et al. [18] solved the structures of $La(OH)SO_4$, $Pr(OH)SO_4$ and $Nd(OH)SO_4$, Jacobson et al. [19] and Feng et al. [20] respectively reported the structures of $Y(OH)SO_4$ and $Ce(OH)SO_4$, Xu et al. detailed the structures of $Eu(OH)SO_4$ and $Dy(OH)SO_4$ [11, 21], and Zehnder et al. investigated the effect of lanthanide contraction on crystal structure of this series of compounds for RE = Pr-Yb lanthanides [22]. It was suggested by

these earlier studies that, although they are all monoclinic ($P2_1/n$ space group), the larger RE^{3+} (RE = La-Gd) and smaller RE^{3+} (RE = Tb-Yb and Y) form two separate types of crystal structures, where the RE^{3+} is 9-fold and 8-fold coordinated by oxygen atoms, respectively. Another difference is that the $RE(OH)SO_4$ of larger RE^{3+} possesses a unit cell accommodating four complete formulas [18, 20, 21, 23] while that of the smaller RE^{3+} has a unit cell containing eight formulas [11, 19]. Zehnder et al. [22] speculated that such a "break" between Gd and Tb is associated with lattice energy and lattice strain.

The family of $RE(OH)SO_4$ compounds were reported to form in the oxide-hydroxide-sulfate reaction system during hydrothermal equilibria study, which employed harsh reaction conditions such as high temperature (≥ 450 °C), high pressure (≥ 120 MPa) and long reaction duration (longer than 6 days) [18, 21, 22]. Our systematic study on the synthesis of $RE_2(OH)_5A{\cdot}nH_2O$ (n ~ 1.5) and $RE_2(OH)_4SO_4{\cdot}nH_2O$ (n = 0 or 2) LREHs clearly manifested the influence of lanthanide contraction and identified that solution pH, aside from temperature, is a decisive factor for the intended compound to be formed, and the results were rationalized by considering cation hydrolysis and coordination competition [7, 8, 24-26]. In view of the previous results, we performed hydrothermal reaction of the $RE(NO_3)_3$-$(NH_4)_2SO_4$-NH_4OH system for the full series of lanthanides (excluding radioactive Pm, including Y) under near-neutral conditions, and phase-pure $RE(OH)SO_4$ was successfully obtained for RE = La-Tb via reaction at the mild temperature of 180 °C for 24 h. The products were characterized in detail to manifest the intrinsic influence of lanthanide contraction on crystal structure, thermal behavior, vibrational property and crystallite morphology. It was clearly shown that

$Tb(OH)SO_4$ is isostructural with its La-Gd analogues instead of the Dy-Yb ones, implying that two types of crystal structures may exist for $Tb(OH)SO_4$ and even $Dy(OH)SO_4$. Furthermore, the pH-, time- and temperature-course of phase and morphology evolution was clarified with RE = Tb for example, and the RE = Eu and Tb compounds were also investigated for their photoluminescence properties.

2. Experimental Section

2.1. Hydrothermal synthesis

Analytical grade $(NH_4)_2SO_4$ and NH_4OH were purchased from Sinopharm Co., Ltd (Shanghai, China), and 99.99% pure $Ce(NO_3)_3·6H_2O$, Pr_6O_{11}, Tb_4O_7 and RE_2O_3 were purchased from Huizhou Ruier Rare-Chem. Hi-Tech. Co. Ltd (Huizhou, China). The rare earth oxides listed above were separately dissolved in a proper amount of HNO_3 to form nitrate solution. Ultra-pure water (resistivity > 18 MΩ·cm) was used throughout the experiments.

In a typical synthesis of $RE(OH)SO_4$, 3.1 mmol of $(NH_4)_2SO_4$ was dissolved in 60 mL aqueous solution containing 3 mmol of RE^{3+} under magnetic stirring, followed by pH adjustment with NH_4OH until the solution changed from clear to cloudy. The resultant mixture was homogenized via constant magnetic stirring for 30 min before being transferred into a Teflon lined stainless steel autoclave (100 mL capacity) for 24 h of reaction in an electric oven preheated at 180 °C. After the reaction, the precipitate was collected via centrifugation, washed with water and ethanol successively, and then dried at 60 °C for 12 h to yield powder products. With RE = Tb for example, a series of experiments were carried out

to investigate the influence of solution pH (6.5-10.0), reaction time, and reaction temperature (70-180 °C).

2.2. Characterization

Phase identification was performed via X-ray diffractometry (XRD, SmartLab, Rigaku, Tokyo, Japan) under 40 kV/200 mA, using nickel-filtered Cu-*K*α radiation (λ = 0.15406 nm) and a scanning speed of 6° 2θ/min. The XRD data for structure analysis were collected via step-scan over the 2θ range of 10-100°, using a step width of 0.02° and a counting time of 10 s per step. Crystal structure refinement was performed by the Rietveld technique as implemented in the TOPAS v4.2 software suite (Bruker, Germany). Thermogravimetry/differential thermal analysis (TG/DTA, Model SETSYS Evolution-16, Setaram, France) was performed at a constant heating rate of 10 °C/min in flowing simulated air (50 mL/min). Fourier transform infrared spectroscopy (FTIR, Nicolet iS5, Thermo Fisher Scientific, Waltham, USA) was conducted using the standard KBr pellet method. Product morphology was analyzed by field emission scanning electron microscopy (FE-SEM, Model JSM-7001F, JEOL, Tokyo) under an acceleration voltage of 15 kV. Photoluminescence and fluorescence decay were analyzed with a Model FP-8600 fluorospectrophotometer (JASCO, Tokyo) equipped with a 60 mm-diameter integrating sphere, using a 150 W xenon lamp for excitation, a slit width of 5 nm, and a scan speed of 500 nm/min.

Results and discussion

3.1 Characterization of the hydrothermal products

Hydrothermal reaction was carried out for the series of lanthanides (excluding radioactive Pm) and Y under 180 °C for 24 h in an attempt to obtain $RE(OH)SO_4$. It was found that, for

different type of RE, the pH value for the transparent RE^{3+} solution to turn turbid (turbidity pH) is different, and the pH gradually decreased from 7.7 to 6.1 as the size of RE^{3+} decreased from La^{3+} to Lu^{3+}, noticing that Y^{3+} and Ho^{3+} are very similar in ionic radius. This is consistent with the fact that smaller RE^{3+} has a stronger hydrolysis capacity due to lanthanide contraction [27]. Fig. 1 shows the XRD patterns of the series of hydrothermal products, togther with the turbidity pH. It can be seen that the La-Tb products (Fig. 1a) conform to the monoclinic $La(OH)SO_4$ standard (PDF No. 04-015-7588), and the diffraction peaks tend to move to larger diffraction angles with decreasing RE^{3+} size. The diffraction pattern of the Dy product basically matches with the $Eu(OH)SO_4$ standard (PDF No. 04-014-5923), except for a diffraction shift towards larger angles and the existence of additional weak peaks (marked with "♦"). This indicates that the Dy product might be a mixture of $Dy(OH)SO_4$ and unknown impurity phase. The diffraction patterns of the RE = Ho-Lu and Y products (Fig. 1b) can not be indexed with any of the RE-containing compounds in the ICDD database or literature, but the coexistence of widened and sharp diffraction peaks indicates that they might be phase mixtures or a single phase of significantly anisotropic crystallite morphology (such as two-dimensional) in each case. As said earlier, the $RE(OH)SO_4$ compounds of lighter (RE = La-Gd) and heavier (RE = Tb-Yb, including Y) lanthanides are separately isostructured and have REO_9 and REO_8 polyhedrons, respectively, although they are all monoclinic and belong to $P2_1/n$ space group [13, 18-20, 22]. Zehnder et al. [22] suggested that the "break" between Gd and Tb is owing to the excessive strain and crystal energy of the REO_9 polyhedron caused by the reduction of RE^{3+} radius. We carefully compared the XRD pattern of the $Tb(OH)SO_4$ prepared in this work with that of the $Tb(OH)SO_4$ reported by Zehnder et al. (PDF No. 04-

018-2414; Fig. S1). The significant differences between the two patterns indicated that the $Tb(OH)SO_4$ of this work belongs to the La-Gd series rather than the Tb-Yb ones and there are two crystal forms for $Tb(OH)SO_4$ and even $Dy(OH)SO_4$ (Fig. 1b).

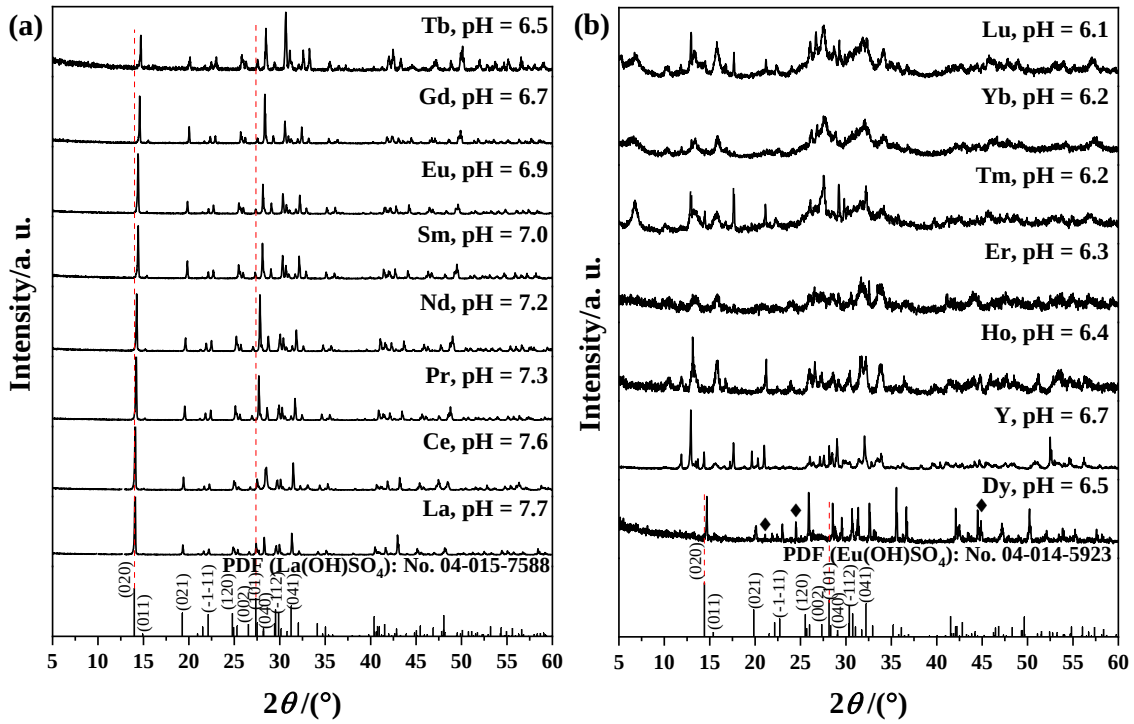

Fig. 1. XRD patterns of the hydrothermal products of RE = La-Tb (a) and RE = Dy-Lu and Y (b), with those of the monoclinic structured $La(OH)SO_4$ (PDF No. 04-015-7588) and $Eu(OH)SO_4$ (PDF No. 04-014-5923) standards included for comparison.

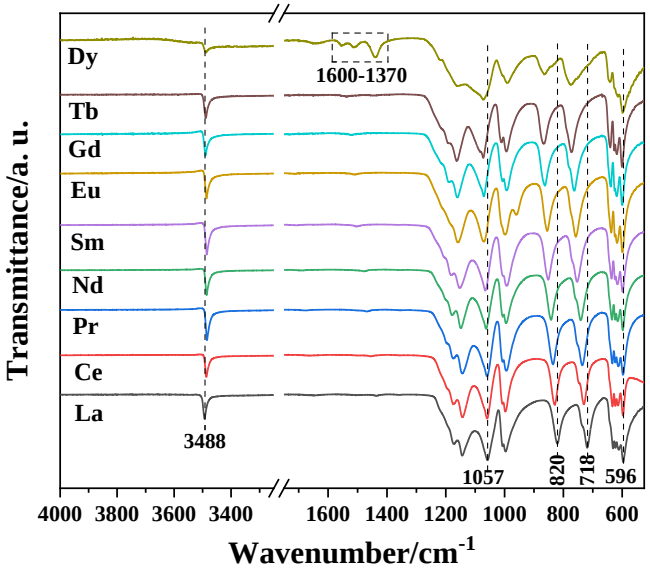

Fig. 2. FTIR spectra of the hydrothermal products for RE = La-Dy.

The stretching vibration of OH^- (ν_1) can also be used to distinguish the two crystal forms,

as it was reported that the ν_1 would be a single state (unimodal, in the regions of ~3455-3505 cm^{-1}) for the REO_9 type and would be a dual state (bimodal, in the regions of ~3455-3505 cm^{-1} and 3540-3570 cm^{-1}) for the REO_8 type [22]. FTIR analysis was thus conducted for the La-Dy products and the resulting spectra are shown in Fig. 2. It is seen that the ν_1 vibration of OH^- in each case is unimodal (~3488 cm^{-1}), which obviously confirms that the as-prepared $RE(OH)SO_4$ (La-Dy) compounds all belong to the REO_9 crystal form. In addition to ν_1, the bending vibration (ν_2) of OH^- was also observed in the region of ~663-906 cm^{-1}. Additionaly, the characteristic vibrations of SO_4^{2-} are well identifiable at ~1001 cm^{-1} (ν_1, medium strong) and in the regions of ~1019-1270 cm^{-1} (ν_3 strong) and 565-653 cm^{-1} (ν_4, strong) [28]. The Dy product differs from the La-Tb ones by showing additional absorptions in the range of ~1370-1600 cm^{-1}. These vibrations, attributable to NO_3^- (from RE nitrate) and CO_3^{2-} (from atmospheric CO_2) [28, 29], may partially reflect the chemical composition of the impurity phase. Shifting of the bending mode (ν_2) of OH^- to a larger wavenumber with decreasing RE^{3+} size is much faster than that of the SO_4^{2-} vibrations, which is owing to higher structure rigidity of the [SO_4] tetrahedron.

In order to clarify structure details, Rietveld refinement of the XRD pattern was conducted for $Tb(OH)SO_4$, using $Eu(OH)SO_4$ (COD-2211386) as initial structure model. The results (Table 1 and Fig. S2) indicated that the compound is single phasic and its diffractions can be readily indexed in the monoclinic unit cell ($P2_1/n$ space group). The results of peak indexation in the range of 2θ = 5-45° are shown in Fig. S3, and Table S1 and Table S2 summarize the derived structure details, including atomic coordinates, *d*-spacing, and Miller index.

Table 1. The results of Rietveld structure refinement for the $Tb(OH)SO_4$ compound.

symmetry	monoclinic
space group	$P2_1/n$
a (Å)	4.3806(1)
b (Å)	12.1729(1)
c (Å)	6.7674(2)
β (°)	106.3967(13)
V (Å^3)	346.19(1)
Z	4
2θ-range (°)	10-100
R_{wp} (%)	9.91
R_{exp} (%)	5.03
R_p (%)	6.82
χ^2	1.97
R_B (%)	1.17

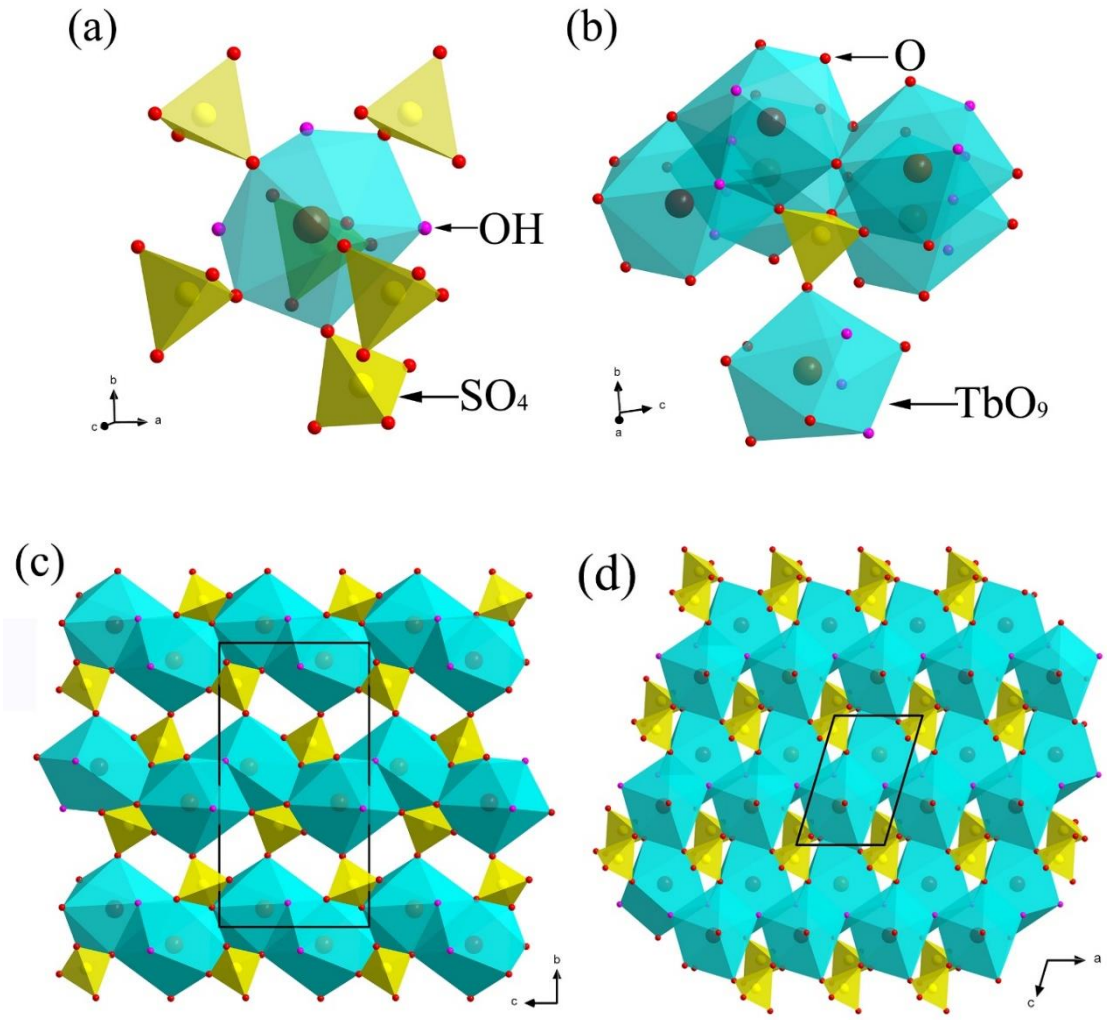

Fig. 3. Schematic illustration of the coordination environment of Tb^{3+} (a), the coordination mode of sulfate group (b), and the crystal structure viewed along axis a (c) and axis b (d) for the $Tb(OH)SO_4$ compound.

Fig. 3 shows the crystal structure and polyhedron geometries of $Tb(OH)SO_4$, which were

visualized by the Diamond software. Similar to $La(OH)SO_4$ [23] and $Eu(OH)SO_4$ [21], the framework of the $Tb(OH)SO_4$ compound features $[TbO_9]$ polyhedron and $[SO_4]$ tetrahedron. Each $[TbO_9]$ is connected to six $[SO_4]$ by sharing vertices, among which five are from the same layer and one from the adjacent layer (Fig. 3a,c). Meanwhile, all the O atoms of the sulfate group take part in Tb coordination, three of which participate in the construction of the same layer by connecting five Tb^{3+} ions and the other one bridges one Tb^{3+} in the adjacent layer along the *b* axis (Fig. 3b,c). The coordination of Tb^{3+} is finally completed by the O atoms from three hydroxide ions, which act as bridging ligands between three Tb^{3+} ions (Fig. 3a,d). The $[TbO_9]$ polyhedrons are connected via alternative edge- and face-sharing to form infinite chains along the *c* axis (Fig. 3c,d), and the chains then form *ac* layers by vertex sharing along the *a* axis (Fig. 3d). The layers confined to *ac* planes are finally tied together by the bridging $[SO_4]$ tetrahedrons along the *b* axis to form a layered crystal structure.

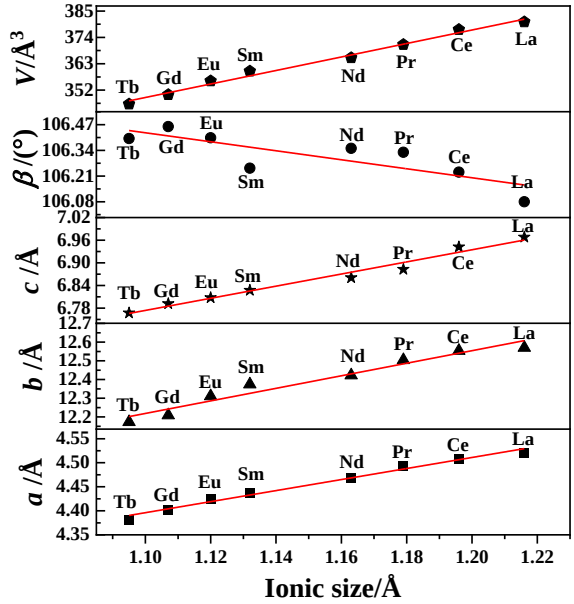

Fig. 4. Correlation of lattice constants (*a*, *b* and *c*), axis angle (β) and cell volume (*V*) with the ionic radius of RE^{3+} (CN = 9).

Fig. 4 shows the lattice parameters derived with Jade 6 software for the series of

$RE(OH)SO_4$, where it is seen that lattice constants (*a*, *b* and *c*) and cell volume (*V*) tend to linearly decrease as the radius of RE^{3+} decreases while axis angle β showed an opposite tendency. The contraction of unit cell explains the diffraction shift of $RE(OH)SO_4$ to higher angles as RE^{3+} size decreases (Fig. 1), which is consistent with lanthanide contraction.

FE-SEM analysis (Fig. 5) demonstrated the La-Tb products are mostly composed of giant laths with a side length up to ~50 μm in each case, which is the typical morphology of $RE(OH)SO_4$ and is consistent with previous reports [13, 30]. Two types of distinctly different particles/crystallites were observed in the Dy product, with the giant laths and flower-like clusters (~2 μm in size) presumbly belonge to $Dy(OH)SO_4$ and the impurity phase, respectively, in accordance with the results of XRD and FTIR analyses (Fig. 1b and Fig. 2). The two-dimensional (2D) growth behavior of the $RE(OH)SO_4$ crystals is an externalization of ther layered crystal structure, which is similar to the situations of SO_4^{2-}-LREH and A^--LREH layered compounds [31, 32].

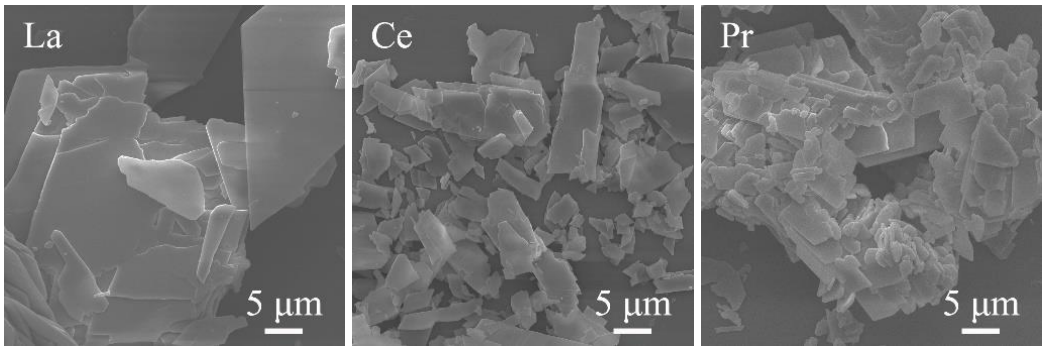

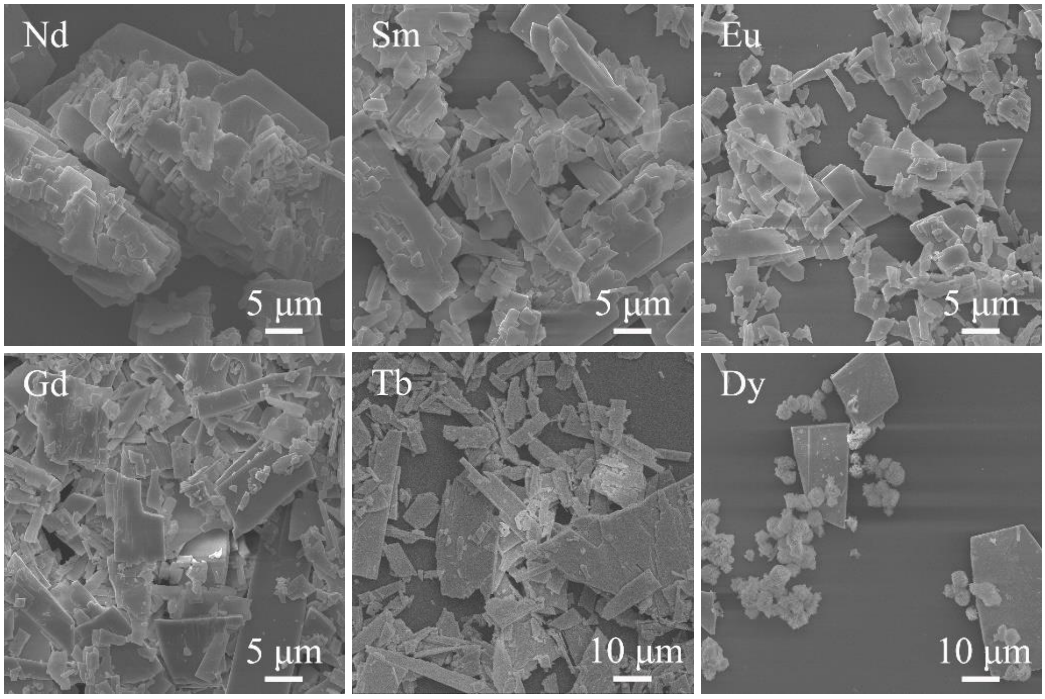

Fig. 5. FE-SEM morphologies of the hydrothermal products for RE = La-Dy.

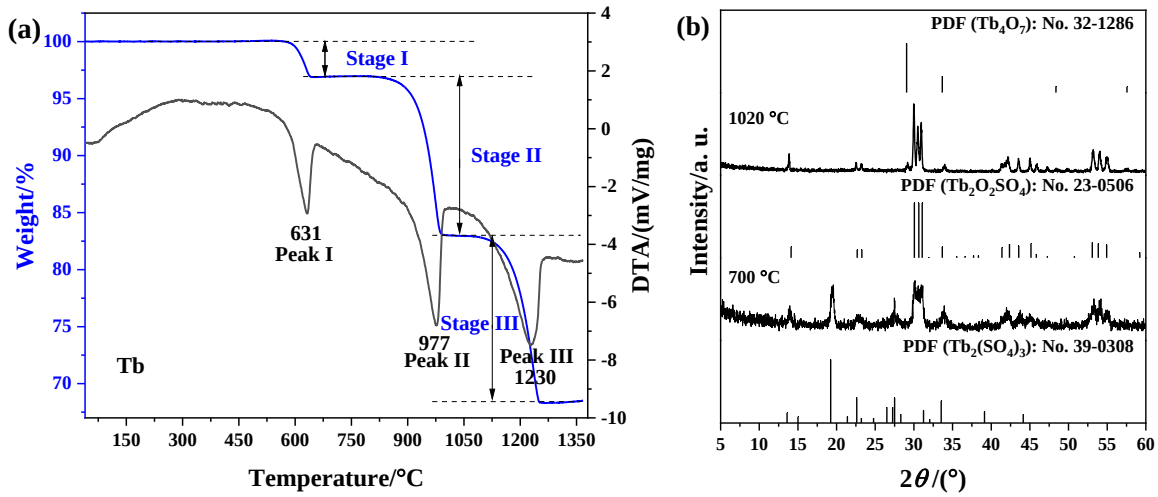

Fig. 6. TG/DTA curves for $Tb(OH)SO_4$ (a) and XRD patterns of the products obtained by calcining $Tb(OH)SO_4$ at different temperatures for 1 h (b).

The thermal behaviors of the series of $RE(OH)SO_4$ were comparatively investigated by TG/DTA in simulated air, and the results are shown in Fig. 6a for the $Tb(OH)SO_4$ representative and in Fig. S4 for the rest. It is seen that thermal decomposition similarly proceeds via three distinct stages (Fig. 6a), and each stage is accompanied by an endothermic peak. The three successive stages correspond to dehydroxylation (removal of OH^-) to form a

nominal composition of $RE_2O(SO_4)_2$, desulfurization of $RE_2O(SO_4)_2$ to yield $RE_2O_2SO_4$, and desulfurization of $RE_2O_2SO_4$ to produce RE oxide, respectively. Noteworthy is that $RE_2O(SO_4)_2$ could be a compound or a mixture of equi-molar $RE_2O_2SO_4$ and $RE_2(SO_4)_3$. For a better understanding, the $Tb(OH)SO_4$ representative was calcined at a temperature (700 °C) covered in stage I for 1 h. XRD analysis (Fig. 6b) found that the product is actually a mixture of $RE_2O_2SO_4$ and $RE_2(SO_4)_3$, indicating that the latter is the actual case. In addition, the product calcined at 1020 °C is mainly composed of $Tb_2O_2SO_4$ (Fig. 6b), indicating that $RE(OH)SO_4$ was indeed converted to $RE_2O_2SO_4$ after stage II. In addition, the weak diffractions characteristic of Tb_4O_7 indicates the commencement of stage III (Fig. 6b), which verifies that stage III indeed corresponds to the conversion of $RE_2O_2SO_4$ to oxide. From the above discussion and the weight loss observed for each stage, the procedure of $RE(OH)SO_4$ decomposition can be detailed as follows: (1) $RE(OH)SO_4 \rightarrow 0.25RE_2O_2SO_4 + 0.25RE_2(SO_4)_3 + 0.5H_2O$ (Stage I); (2) $RE_2(SO_4)_3 \rightarrow RE_2O_2SO_4 + 2SO_3$ (Stage II); (3) $RE_2O_2SO_4 \rightarrow$ RE oxide + SO_3 (Stage III). The decomposition data are tabulated in Table 2 for the entire series of $RE(OH)SO_4$ except for RE = Ce. The Ce sample was not discussed here because it is easily oxidized to CeO_2 in air. Since the thermal stability of $RE_2O_2SO_4$ increases with increasing RE^{3+} radius [7, 33], the La-Nd samples showed the first two stages of decomposition in the measured temperature range of 30-1380 °C while a complete three-stage decomposition was observed for the Sm-Tb samples. In the latter case, the shifting towards a higher temperature of peak III with increasing RE^{3+} size well corresponds to previous reports [7, 33]. Besides, the tending to be higher temperature of dehydroxylation with decreasing

RE^{3+} radius (peak I, Table 2), as observed for SO_4^{2-}-LREH and $RE_2(OH)_2CO_3SO_4 \cdot nH_2O$ (REOCSH, RE = Gd-Lu) [7, 8, 34], is in line with the Pearson hard-soft-acid-base (HSAB) theory by considering lanthanide contraction, though the occurrence temperature of peak II did not show a clear trend (Table 2). The good correspondence of the observed (Table 2) and theoretical (Table S3) weight losses further confirmed the proposed decomposition procedures.

Table 2 A summary of thermal decomposition data for the $RE(OH)SO_4$ compounds (RE = La-Tb, excluding Ce) up to 1380 °C

RE	Peak I (°C)	Peak II (°C)	Peak III (°C)	Weight loss I (%)	Weight loss II (%)	Weight loss III (%)	Sum of weight loss (%)
La	607	1061	---	3.49	15.10	Incomplete	18.59
Pr	598	993	---	3.43	15.00	Incomplete	18.43
Nd	606	1004	---	3.40	14.81	Incomplete	18.21
Sm	606	996	1316	3.39	14.71	14.58	32.68
Eu	608	948	1295	3.34	14.38	14.41	32.13
Gd	621	1019	1290	3.23	14.26	14.29	31.78
Tb	631	977	1230	3.29	14.57	13.13	30.99

3.2 The effect of solution pH and reaction temperature on the phase and morphology evolution of $RE(OH)SO_4$

Up to now, a systematic study on the effects of hydrothermal parameters such as soution pH and temperature on the synthesis of $RE(OH)SO_4$ is still lacking. Therefore, we conducted a detailed investigation with RE = Tb as a representative. Fig. 7 shows the XRD patterns of the products obtained via reaction at 180 °C under different pH values. It can be seen that in the wide pH range of 6.5-10, $Tb(OH)SO_4$ is only obtainable at pH = 6.5 and no precipitate was obtained at pH ≤ 6. The pH = 7 product is an unknown phase, and FTIR analysis (Fig. S5) showed that it contains SO_4^{2-}, OH^-, NH_4^+ and H_2O. The pH = 8 and 9 products are SO_4^{2-}-LTbH ($Tb_2(OH)_4SO_4$), and their FTIR spectra (Fig. S5) indeed showed the typical vibrations of SO_4^{2-}-LTbH [8]. The pH = 10 product is also an unknown phase, and FTIR analysis identified the exixtence of SO_4^{2-}, OH^-, NH_4^+ and H_2O, but the vibrations of OH^- is more

abundant. Although the $RE(NO_3)_3$-$(NH_4)_2SO_4$-NH_4OH reaction system is simple, the above results indicated that the phase evolution of hydrothermal product is very rich and complicated. A weakly acidic environment is conducive to $Tb(OH)SO_4$ formation, which is similar to the cases of REOCSH ($RE_2(OH)_2CO_3SO_4 \cdot nH_2O$; pH = 6) [34, 35]. Since the OH^-/RE^{3+} molar ratio (1:1) of $Tb(OH)SO_4$ is the same as that of REOCSH but is lower than that (2:1) of SO_4^{2-}-LREH, it is thus understandable in view of coordination competition that a higher solution pH is required for SO_4^{2-}-LTbH to form. FE-SEM analysis found that the pH = 7 product is composed of sheets with a length of ~1-3 μm and a width of ~100-500 nm, the pH = 8 and 9 products (SO_4^{2-}-LTbH) contian blocks of ~10-30 μm in length and ~5-10 μm in width, and the pH = 10 product consists of needle-like objects of bout ~5-20 μm long. The morphology of $Tb(OH)SO_4$ (pH = 6.5) is the same as that in Fig. 5 and is not detailed here. The pH = 7 and 10 products could both be single phasic, as inferred from their uniform morphologies, though more studies are needed for clarification.

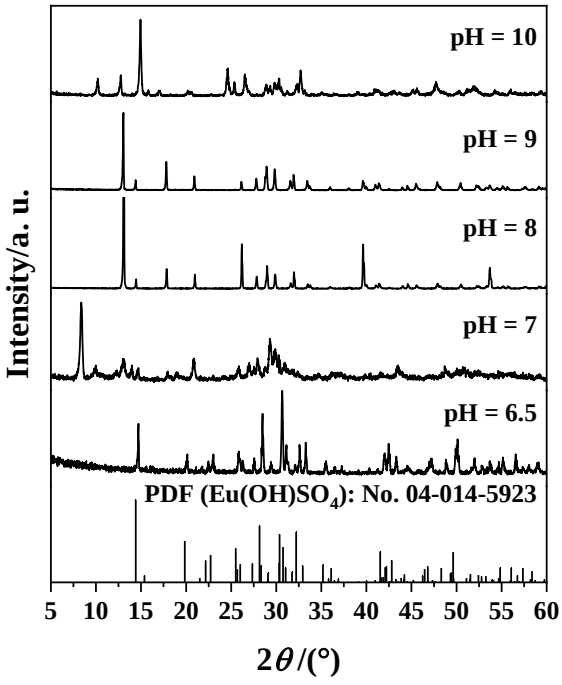

Fig. 7. XRD patterns of the products obtained under 180 °C and different solution pH.

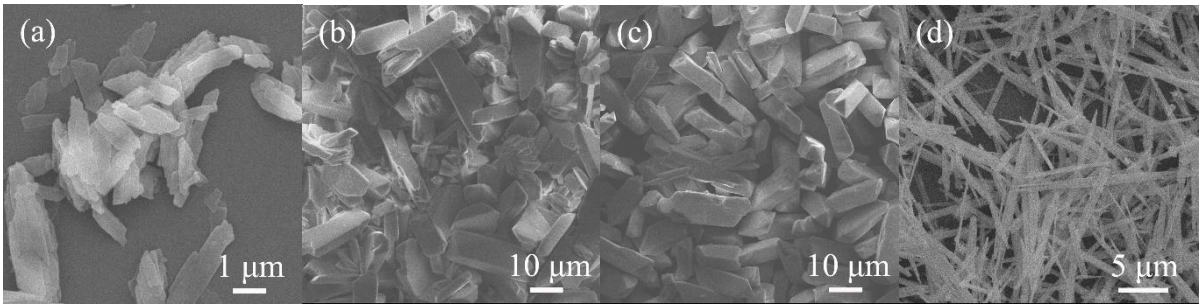

Fig. 8. FE-SEM morphologies of the products obtained via reaction at 180 °C and the different solution pH values of 6 (a), 7 (b), 8 (c) and 10 (d).

To better understand $Tb(OH)SO_4$ formation, we tracked the time-course phase and morphology evolution under the fixed reaction conditions of 180 °C and pH = 6.5. As shown in Fig. 9, the 35 min product (Fig. 9a) is a fibrous aggregate, which turned into flower-like clusters with a diameter of ~5 μm when the reaction time reached 1 h (Fig. 9b). XRD analysis (Fig. S6) showed the 35 min product is amorphous while the 1 h one is very similar to that of the aforesaid pH = 7 product (Fig. 7). The primary architecture units of the flower-like clusters (the inset in Fig. 9b) are also consistent with the lamellar morphology of the pH = 7 product, indicating that they might be the same phase. After a duration of 2 h, the flower-like clusters were observed to further nucleate and grow, with the individual particles reached up to ~10 μm in diameter (Fig. 9c). After 4 h of reaction, the flower-like clusters were found to coexist with irregular lath-like particles, where the size of the former hardly changed but the length of the latter reached ~10 μm (Fig. 9d). As the lath-like morphology is typical of $RE(OH)SO_4$ in this work (Fig. 5), the appearance of mixed morphologies thus indicates that $Tb(OH)SO_4$ was crystallized through a typical dissolution-reprecipitation (DR) process. The already quite big $Tb(OH)SO_4$ particles/crystallites in the 4 h product may imply a fast growth following nucleation. The XRD pattern (Fig. S6) of the 2 h product is similar to that of the 4 h product, where the weak peak at $2\theta = 14.52°$ corresponds to the (020) plane of $Tb(OH)SO_4$.

The content of $Tb(OH)SO_4$ in the 6 h product increased significantly, and the observed breakage of flower-like clusters was resulted from dissolution (Fig. 9e). This is because the nucleation and growth of $Tb(OH)SO_4$ during the DR process continuously consumes solutes, which drives the earlier precipitate (clusters) to dissolve. After 10 h of reaction, the $Tb(OH)SO_4$ microcrystals grew further, and giant laths of ~60 μm were formed (Fig. 9f). The relative content changes of the flower-like clusters and $Tb(OH)SO_4$ during the whole DR process are consistent with the results of XRD analysis (Fig. S6).

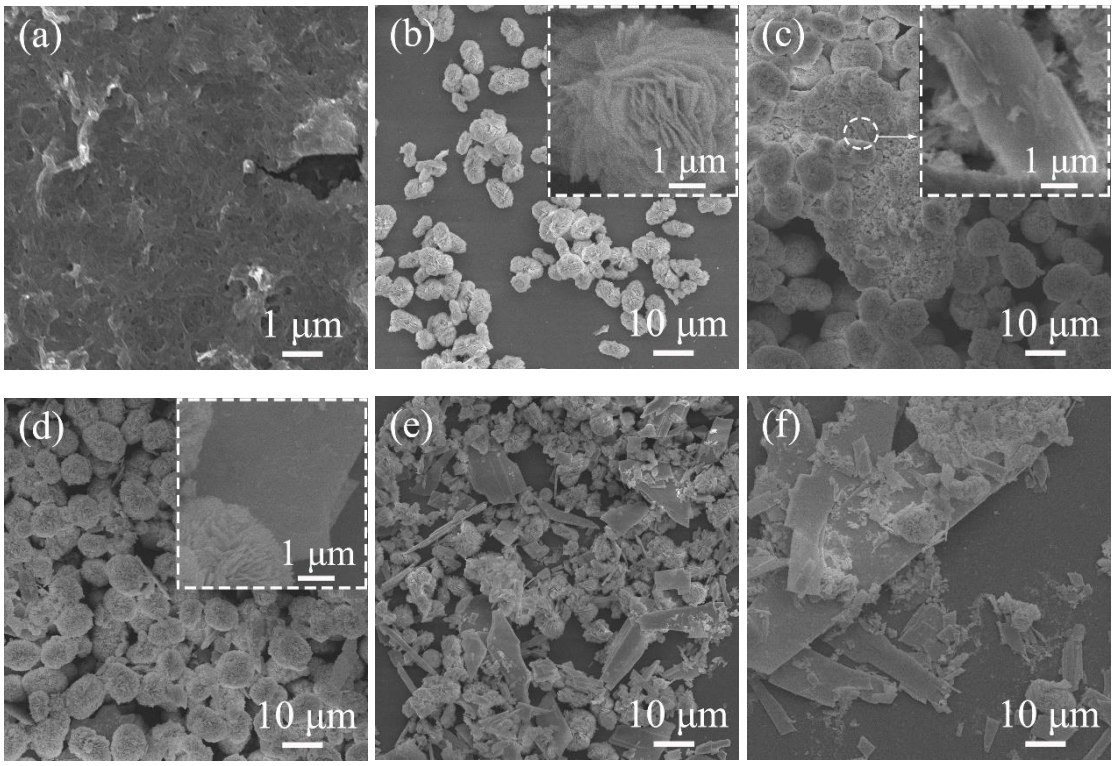

Fig. 9. FE-SEM morphologies of the products obtained by 180 °C hydrothermal reaction under pH = 6.5 for 35 min (a), 1 h (b), 2 h (c), 4 h (d), 6 h (e) and 10 h (f). The insets in (b), (c) and (d) are closer views.

As aforesaid, $Tb(OH)SO_4$ was crystallized through a DR process, which requires the energy provided by the thermal field to cross a certain barrier. Therefore, hydrothermal temperature would have an important influence on $Tb(OH)SO_4$ formation. We thus tracked the temperature-course of phase and morphology evolution. As shown in Fig. 10, the 70 and

100 °C products are amorphous, and FE-SEM analysis showed that they are irregular aggregates (Fig. S7a, b). The diffraction pattern of the 120 °C product (Fig. 10) is similar to those of the aforesaid pH = 7 (Fig. 7) and 1 h (Fig. S6) products, except that the diffraction peaks are sharper. Different from the 1 h product (flower-like clusters, Fig. 9b), the 120 °C product is composed of spheroidal particles of ~50 μm and also a small amount of aggregates (Fig. S7c). The primary architectural unit of the spheroids is significantly larger and wider than that of the 1 h product, which is consistent with the sharper diffraction of the 120 °C product. The 150 °C product only showed weak (020) diffraction of $Tb(OH)SO_4$ (Fig. 10), and largely contains flower-like clusters (~10 μm), together with some $Tb(OH)SO_4$ laths (Fig. S7d), indicating that the DR process only partially occurred. Therefore, it can be concluded that at least ~180 °C is needed for the DR process to complete.

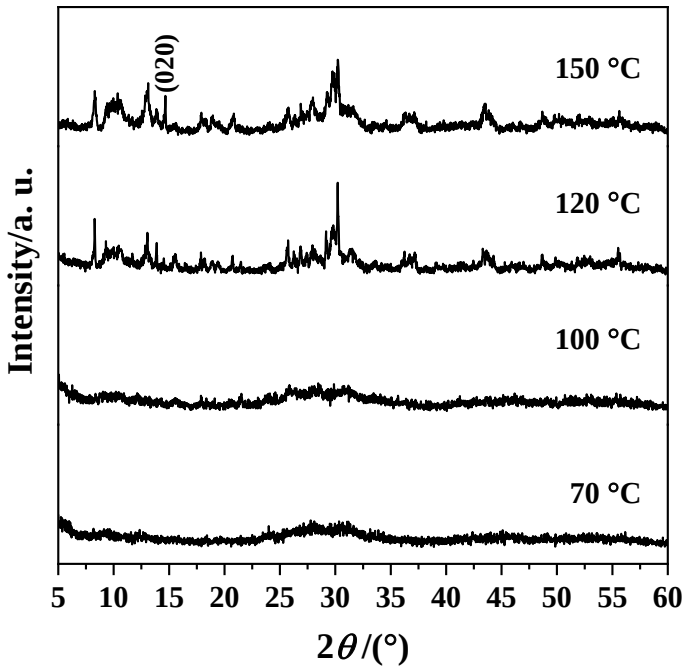

Fig. 10. The XRD patterns of the products obtained at different hydrothermal temperatures.

3.3 Photoluminescence properties of Eu(OH)SO₄ and Tb(OH)SO₄

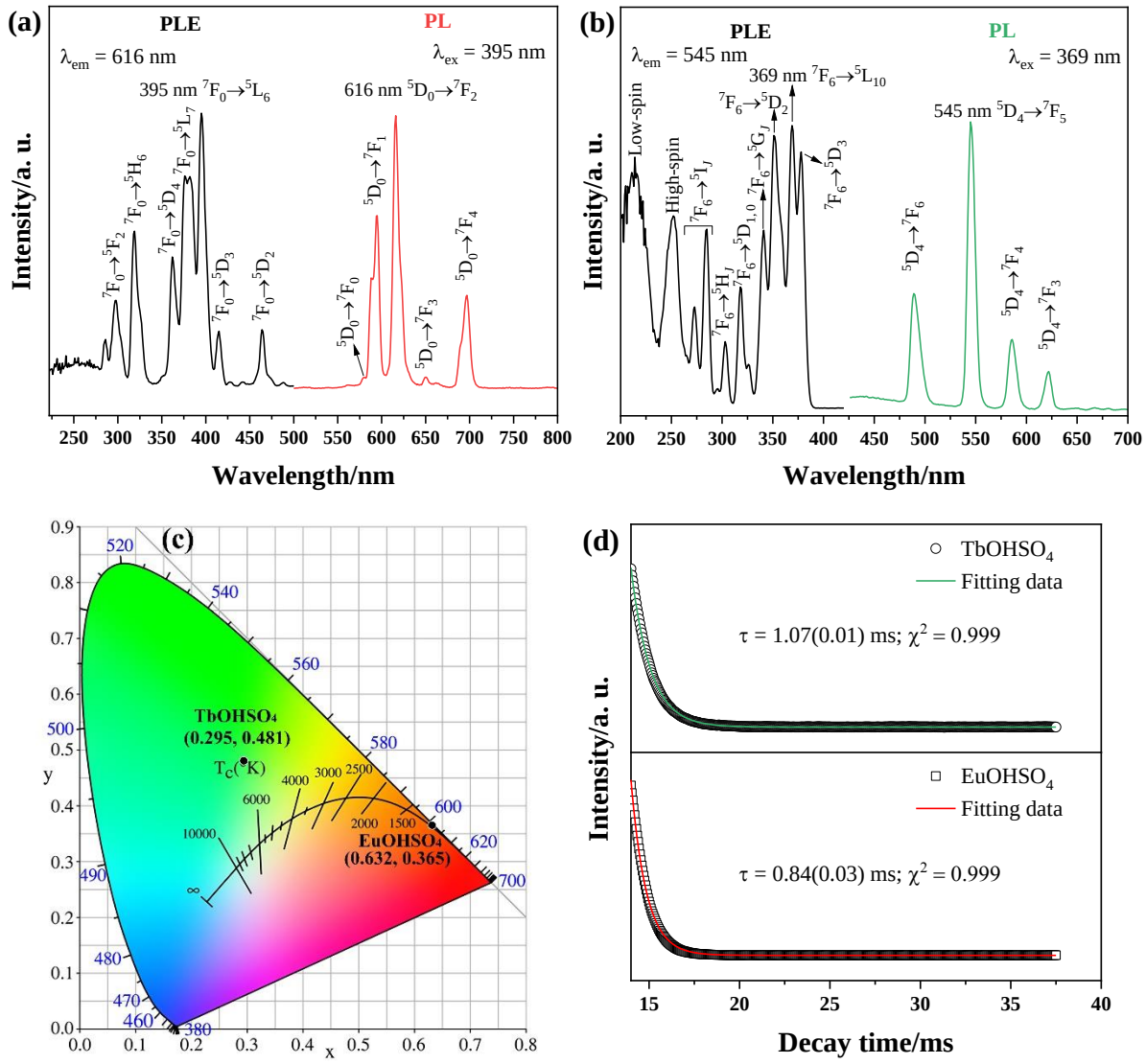

Fig. 11. PLE and PL spectra of the $Eu(OH)SO_4$ (a) and $Tb(OH)SO_4$ (b) compounds, together with the CIE chromaticity diagram (c) and fluorescence decay behaviors (d) of luminescence.

Fig. 11 shows the photoluminescence excitation (PLE) and emission (PL) spectra of the $Eu(OH)SO_4$ and $Tb(OH)SO_4$ compounds. Noteworthy is that the other $RE(OH)SO_4$ products are not luminescent even though their RE^{3+} ions are optically active (RE = Ce, Pr, Sm, Gd, Dy). For $Eu(OH)SO_4$ (Fig. 11a), the PLE spectrum obtained by monitoring the 616 nm red emission ($^5D_0 \rightarrow {}^7F_2$ transition) displayed a series of sharp lines in the ~270-500 nm region for the intra-4*f*^{6} transitions of Eu^{3+} [36-38], with the $^7F_0 \rightarrow {}^5L_6$ excitation at ~395 nm being

the strongest. The PL spectrum obtained under UV excitation at 395 nm exhibited the typical $^5D_0 \rightarrow {}^7F_J$ (J = 0-4) emissions of Eu^{3+} at 579, 595, 616, 651 and 697 nm, as labeled in the figure, with the $^5D_0 \rightarrow {}^7F_2$ red emission (616 nm) being the most prominent. Since Eu^{3+} would occupy low-symmetric C_1 sites in $Eu(OH)SO_4$, the parity forbidden $^5D_0 \rightarrow {}^7F_2$ electric dipole transition is stronger than the parity allowed $^5D_0 \rightarrow {}^7F_1$ magnetic dipole transition [39, 40]. For $Tb(OH)SO_4$ (Fig. 11b), the PLE spectrum recorded by monitoring the 545 nm green emission ($^5D_4 \rightarrow {}^7F_5$ transition) of Tb^{3+} contains two broad bands centered at ~214 and 252 nm for the spin-allowed (low-spin) and spin-forbidden (high-spin) $4f^8 \rightarrow 4f^75d^1$ intra-configurational transitions of Tb^{3+} [41], respectively, and also a series of sharp peaks in the longer wavelength region for the intra-$4f^8$ transitions of Tb^{3+}, as assigned in the figure, with the $^7F_6 \rightarrow {}^5L_{10}$ transition at ~369 nm being the most prominent [42, 43]. Under 369 nm excitation, $Tb(OH)SO_4$ showed luminescence via transition from the $^5D_4$ excited state to ^7F_J (J = 3-6) ground multiples of Tb^{3+}, as indicated in the figure, with the $^5D_4 \rightarrow {}^7F_5$ green emission at ~545 nm being the strongest. The Eu and Tb compounds were analyzed from their PL spectra to have Commission Internationale de L'Eclairage (CIE) chromaticity coordinates (Fig. 11c) of around (0.632, 0.365) and (0.295, 0.481), typical of orange red and green colors, respectively. Fluorescence decay analysis found that the main luminescence of Eu^{3+} (λ_{em} = 616 nm, λ_{ex} = 395 nm) and Tb^{3+} (λ_{em} = 545 nm, λ_{ex} = 369 nm) both decreased in a single exponential manner (Fig. 11d), and have lifetime values of 0.84±0.03 and 1.07±0.01 ms, respectively.

4. Conclusion

A family of $RE(OH)SO_4$ layered compounds (RE = La-Tb lanthanides) were successfully obtained via mild hydrothermal reaction at 180 °C for 24 h. The solution pH for $RE(OH)SO_4$ formation was found to decreass with decreasing ionic radiu of RE^{3+}. The Tb compound was analyzed to be isostructural with its La-Gd analogues rather than the reportedly Dy-Yb ones, and it has a monoclinic unit cell ($P2_1/n$ space group) of a = 4.3806 Å, b = 12.1729 Å, c = 6.7674 Å and β = 106.3967°, where Tb^{3+} is 9-fold coordinated. An increasing temperature of dehydroxylation and a decreasing temperature of complete desulfurization were observed at a smaller RE^{3+}. Investigation of the time-course and temperature-course of phase/morphology evolution showed that $RE(OH)SO_4$ was formed via a typical dissolution-reprecipitation process. The Eu and Tb compounds showed red (616 nm) and green (545 nm) emissions upon UV exciation, with fluorescence lifetimes of ~0.84 and 1.07 ms and chromaticity coordinates of around (0.632, 0.365) and (0.295, 0.481), respectively.

Acknowledgements

This work was supported in part by the National Natural Science Foundation of China (Grant No. 52172112, 51972047 and 52371057).

References

[1] J.M. Haschke, Preparation, phase equilibriums, crystal chemistry, and some properties of lanthanide hydroxide nitrates, Inorg. Chem., 13 (1974) 1812-1818.
[2] R.A. Zehnder, D.L. Clark, B.L. Scott, R.J. Donohoe, P.D. Palmer, W.H. Runde, D.E. Hobart, Investigation of the structural properties of an extended series of lanthanide bis-hydroxychlorides $Ln(OH)_2Cl$ (Ln = Nd−Lu, except Pm and Sm), Inorg. Chem., 49 (2010) 4781-4790.
[3] Y. Song, M. Luo, C. Lin, N. Ye, Structural modulation of nitrate group with cations to affect SHG responses in $RE(OH)_2NO_3$ (RE = La, Y, and Gd): New polar materials with large NLO effect after adjusting pH values of reaction systems, Chem. Mater., 29 (2017) 896-903.

[4] F. Gándara, J. Perles, N. Snejko, M. Iglesias, B. Gómez-Lor, E. Gutiérrez-Puebla, M.Á. Monge, Layered rare-earth hydroxides: A class of pillared crystalline compounds for intercalation chemistry, Angew. Chem. Int. Ed. , 45 (2006) 7998-8001.
[5] F. Geng, Y. Matsushita, R. Ma, H. Xin, M. Tanaka, F. Izumi, N. Iyi, T. Sasaki, General synthesis and structural evolution of a layered family of $Ln_8(OH)_{20}Cl_4 \cdot nH_2O$ (Ln = Nd, Sm, Eu, Gd, Tb, Dy, Ho, Er, Tm, and Y), J. Am. Chem. Soc., 130 (2008) 16344-16350.
[6] Q. Zhu, X. Wang, J.-G. Li, Recent progress in layered rare-earth hydroxide (LRH) and its application in luminescence, J. Adv. Ceram., 6 (2017) 177-186.
[7] X. Wang, J.-G. Li, M.S. Molokeev, X. Wang, W. Liu, Q. Zhu, H. Tanaka, K. Suzuta, B.-N. Kim, Y. Sakka, Hydrothermal crystallization of a $Ln_2(OH)_4SO_4 \cdot nH_2O$ layered compound for a wide range of Ln (Ln = La–Dy), thermolysis, and facile transformation into oxysulfate and oxysulfide phosphors, RSC Adv., 7 (2017) 13331-13339.
[8] X. Wang, M.S. Molokeev, Q. Zhu, J.-G. Li, Controlled hydrothermal crystallization of anhydrous $Ln_2(OH)_4SO_4$ (Ln=Eu–Lu, Y) as a new family of layered rare earth metal hydroxides, Chem. Eur. J., 23 (2017) 16034-16043.
[9] J. Liang, R. Ma, F. Geng, Y. Ebina, T. Sasaki, $Ln_2(OH)_4SO_4 \cdot nH_2O$ (Ln = Pr to Tb; $n \sim 2$): A new family of layered rare-earth hydroxides rigidly pillared by sulfate ions, Chem. Mater., 22 (2010) 6001-6007.
[10] M.S. Wickleder, Inorganic lanthanide compounds with complex anions, Chem. Rev., 102 (2002) 2011-2088.
[11] Y. Xu, S. Ding, X. Zheng, Hydrothermal synthesis, crystal structure and properties of 2-D and 3-D lanthanide sulfates, J. Solid State Chem., 180 (2007) 2020-2025.
[12] Z. Han, Y. Qian, J. Yang, G.Q. Lu, Soft solution processing of cerium hydroxysulfate powders with different morphologies, J. Mater. Chem., 13 (2003) 150-153.
[13] Z. Han, C. Zhong, J. Cao, S. Yu, K. Tang, H. Zhao, Y. Qian, Hydrothermal synthesis and characterization of $La_{1-x}Ce_xOHSO_4$ phosphors, J. Cryst. Growth, 222 (2001) 528-533.
[14] J. Dong, X. Wang, H. Xiong, H. Song, R. Wu, S. Gan, A novel synthetic route towards monodisperse yttrium hydroxide fluoride by anion exchange and luminescence properties, Opt. Laser Technol., 111 (2019) 372-379.
[15] S. Huang, Z. Wang, Q. Zhu, X. Shi, X. Wang, X. Li, X. Sun, J.-G. Li, A new protocol for templated synthesis of YVO_4:Ln luminescent crystallites (Ln=Eu, Dy, Sm), J. Alloys Compd., 776 (2019) 773-781.
[16] X. Wang, P. Du, W. Liu, S. Huang, Z. Hu, Q. Wang, J.-G. Li, Organic-free direct crystallization of t-$LaVO_4$:Eu nanocrystals with favorable luminescence for LED lighting and optical thermometry, J. Mater. Res. Technol., 9 (2020) 13264-13273.
[17] X. Wang, X. Feng, M. Sun, B. Wang, J. Wang, J.-G. Li, Synthesis of multi-type rare earth compounds with $RE(OH)SO_4$ as a new sacrificial-template and photoluminescence, J. Asian Ceram. Soc., 10 (2022) 575-582.
[18] J.M. Haschke, Hydrothermal equilibria and crystal chemistry of phases in the oxide-hydroxide-sulfate systems of La, Pr, and Nd, J. Solid State Chem., 73 (1988) 71-79.
[19] X. Wang, L. Liu, K. Ross, A.J. Jacobson, Synthesis and crystal structures of yttrium sulfates $Y(OH)(SO_4)$, $Y(SO_4)F$, $YNi(OH)_3(SO_4)$-II and $Y_2Cu(OH)_3(SO_4)_2F \cdot H_2O$, Solid State Sci., 2 (2000) 109-118.

[20] Y. Yang, L.-H. Zhu, M.-H. Zeng, X.-L. Feng, Cerium(III) hydroxide sulfate, $Ce(OH)SO_4$, Acta Crystallogr., Sect. E: Struct. Rep. Online, 61 (2005) i41-i43.
[21] S.-H. Ding, X.-C. Sun, Y.-L. Zhu, Q. Chen, Y. Xu, Europium(III) sulfate hydroxide, Acta Crystallogr., Sect. E: Struct. Rep. Online, 62 (2006) i269-i271.
[22] R.A. Zehnder, C.S. Wilson, H.T. Christy, K.S. Harris, V. Chauhan, V. Schutz, M. Sullivan, M. Zeller, F.R. Fronczek, J.A. Myers, K. Dammann, J. Duck, P.M. Smith, A. Okuma, K. Johnson, R. Sovesky, C. Stroudt, R.A. Renn, Effect of inclining strain on the crystal lattice along an extended series of lanthanide hydroxysulfates $Ln(OH)SO_4$ (Ln = Pr−Yb, except Pm), Inorg. Chem., 50 (2011) 836-846.
[23] Q. Zhang, C. Lu, W. Yang, S. Chen, Y. Yu, Hydrothermal syntheses and crystal structures of two lanthanum compounds $La(OH)SO_4$ and $LaO(NO_3)$, Inorg. Chem. Commun., 7 (2004) 889-892.
[24] J.-G. Li, J. Li, X. Wang, Q. Zhu, X. Li, B.N. Kim, X. Sun, Two-step crystallization of a phase-pure $Ln_2(OH)_5NO_3{\cdot}nH_2O$ layered compound for the smallest Ln ions of Tm, Yb and Lu, anion exchange, and exfoliation, Dalton Trans, 46 (2017) 12683-12691.
[25] Q. Zhu, J.-G. Li, R. Ma, T. Sasaki, X. Yang, X. Li, X. Sun, Y. Sakka, Well-defined crystallites autoclaved from the nitrate/NH_4OH reaction system as the precursor for $(Y,Eu)_2O_3$ red phosphor: Crystallization mechanism, phase and morphology control, and luminescent property, J. Solid State Chem., 192 (2012) 229-237.
[26] X. Wu, J.-G. Li, Q. Zhu, W. Liu, J. Li, X. Li, X. Sun, Y. Sakka, One-step freezing temperature crystallization of layered rare-earth hydroxide ($Ln_2(OH)_5NO_3{\cdot}nH_2O$) nanosheets for a wide spectrum of Ln (Ln = Pr-Er, and Y), anion exchange with fluorine and sulfate, and microscopic coordination probed via photoluminescence, J. Mater. Chem. C, 3 (2015) 3428-3437.
[27] R.L. Rich, Inorganic reactions in water, Springer-Verlag, Berlin Heidelberg, 2007.
[28] J.A. Gadsden, Infrared spectra of minerals and related inorganic compounds, Butterworth, London, 1975.
[29] A. Hezel, S.D. Ross, Forbidden transitions in the infra-red spectra of tetrahedral anions—IV. The vibrational spectra (4000-400 cm^{-1}) of some cobalt (III) sulphato- and phosphato-complexes, Spectrochem. Acta, 24 (1968) 985-992.
[30] X. Wang, J.-G. Li, M.S. Molokeev, Q. Zhu, X. Li, X. Sun, Layered hydroxyl sulfate: Controlled crystallization, structure analysis, and green derivation of multi-color luminescent $(La,RE)_2O_2SO_4$ and $(La,RE)_2O_2S$ phosphors (RE = Pr, Sm, Eu, Tb, and Dy), Chem. Eng. J., 302 (2016) 577-586.
[31] F. Geng, H. Xin, Y. Matsushita, R. Ma, M. Tanaka, F. Izumi, N. Iyi, T. Sasaki, New layered rare-earth hydroxides with anion-exchange properties, Chem. Eur. J., 14 (2008) 9255-9260.
[32] Q. Zhu, J.-G. Li, C. Zhi, X. Li, X. Sun, Y. Sakka, D. Golberg, Y. Bando, Layered rare-earth hydroxides (LRHs) of $(Y_{1-x}Eu_x)_2(OH)_5NO_3{\cdot}nH_2O$ (x = 0−1): Structural variations by Eu^{3+} doping, phase conversion to oxides, and the correlation of photoluminescence behaviors, Chem. Mater., 22 (2010) 4204-4213.
[33] M. Machida, K. Kawamura, K. Ito, K. Ikeue, Large-capacity oxygen storage by lanthanide oxysulfate/oxysulfide systems, Chem. Mater., 17 (2005) 1487-1492.

[34] F. Li, Z. Song, Z. Pan, S. Feng, Q. Zhu, J.-G. Li, Crystallization of $RE_2(OH)_2CO_3SO_4 \cdot nH_2O$ as a new family of layered hydroxides (RE = Gd−Lu lanthanides and Y), derivation of $RE_2O_2SO_4$, photoluminescence and optical thermometry, J. Rare Earths, (2023), https://doi.org/10.1016/j.jre.2023.07.008.
[35] F. Li, S. Feng, Z. Pan, Q. Zhu, X. Sun, J.-G. Li, Controlled preparation of $Gd_2O_2SO_4:Eu^{3+}$ monospheres via hydrothermal precursor engineering for enhanced photoluminescence, Adv. Powder Technol., 34 (2023) 104224.
[36] F. Li, J.-G. Li, Q. Zhu, EDTA-promoted aliovalent Eu^{3+} doping of $Sr_5(PO_4)_3F$ apatite, growth behavior and luminescence, Opt. Mater., 101 (2020) 109765.
[37] S.S. Babu, P. Babu, C.K. Jayasankar, W. Sievers, T. Tröster, G. Wortmann, Optical absorption and photoluminescence studies of Eu^{3+}-doped phosphate and fluorophosphate glasses, J. Lumin., 126 (2007) 109-120.
[38] Y. Huang, J. Liu, W. Zhao, J. Yu, H. Zhou, Y. Cao, B. Hao, J. Liu, Y. Zhao, X. Mo, Synthesis, structure and luminescence properties of a novel red fluorescent material $Ba_2MgB_2O_6:Eu^{3+}$, Ceram. Int., 49 (2023) 29607-29613.
[39] R. Gopal, J. Manam, The photoluminescence and Judd-Ofelt investigations of UV, near-UV and blue excited highly pure red emitting $BaWO_4$: Eu^{3+} phosphor for solid state lighting, Ceram. Int., 49 (2023) 28118-28129.
[40] F. Li, M. Jin, Z. Li, X. Wang, Q. Zhu, J.-G. Li, Vertically aligned $Gd_2O_2SO_4$:Ln and Gd_2O_2S:Ln luminescent films with super-hydrophobicity via a novel precursor route (Ln = Pr, Eu, Tb), Appl. Surf. Sci., 609 (2023) 155323.
[41] M. Sen, R. Shukla, N. Pathak, V. Bhasin, S.N. Jha, D. Bhattacharyya, V. Sathian, P. Chaudhury, A.K. Tyagi, $Al_5BO_9:Tb^{3+}$: Synthesis, structural characterization and thermoluminescence dosimetry studies for high intensity thermal neutron beams, Ceram. Int., 49 (2023) 33358-33368.
[42] Y.-C. Li, Y.-H. Chang, Y.-S. Chang, Y.-J. Lin, C.-H. Laing, Luminescence and energy transfer properties of Gd^{3+} and Tb^{3+} in $LaAlGe_2O_7$, J. Phys. Chem. C, 111 (2007) 10682-10688.
[43] W. Huang, Z. Wen, L. Li, G.A. Ashraf, L. Chen, L. Lei, H. Guo, X. Li, Photoluminescence and X-ray excited scintillating properties of Tb^{3+}-doped borosilicate aluminate glass scintillators, Ceram. Int., 48 (2022) 17178-17184.